ACS APPLIED MATERIALS & INTERFACES

Research Article

www.acsami.org

Eradication of *Plasmodium falciparum* from Erythrocytes by Controlled Reactive Oxygen Species via Photodynamic Inactivation Coupled with Photofunctional Nanoparticles

Kang-Kyun Wang,[†,∥] Jin Woo Jang,[‡,∥] Eon Pil Shin,[†,∥] Hyung Wan Song,[†,∥] Jeong Wook Hwang,[†] Young Keun Kim,[§] Chae Seung Lim,[*,‡] and Yong-Rok Kim[*,†]

[†]Department of Chemistry, Yonsei University, Seoul 03722, Republic of Korea

[‡]Department of Laboratory Medicine, Korea University Guro Hospital, Seoul 08308, Republic of Korea

[§]Department of Materials Science and Engineering, Korea University, Seoul 02841, Republic of Korea

ABSTRACT: We investigated the antimalarial effect of photodynamic inactivation (PDI) coupled with magnetic nanoparticles (MNPs) as a potential strategy to combat the emergence of drug-resistant malaria and resurgence of malaria after treatment. Because the malarial parasite proliferates within erythrocytes, PDI agents need to be taken up by erythrocytes to eradicate the parasite. We used photofunctional MNPs as the PDI agent because nanosized particles were selectively taken up by Plasmodium-infected erythrocytes and remained within the intracellular space due to the enhanced permeability and retention effect. Also, the magnetism of Fe_3O_4 nanoparticles can easily be utilized for the collection of photofunctional nanoparticles (PFNs), and the uptaken PFNs infected the erythrocytes after photodynamic treatment with external magnetics. Photofunctionality was provided by a photosensitizer, namely, pheophorbide A, which generates reactive oxygen species (ROS) under irradiation. PAs were covalently bonded to the surface of the MNPs. The morphology and structural characteristics of the MNPs were investigated by scanning electron microscopy and X-ray diffraction (XRD), whereas the photophysical properties of the PFNs were studied with Fourier transform infrared, absorption, and emission spectroscopies. Generation of singlet oxygen, a major ROS, was directly confirmed with time-resolved phosphorescence spectroscopy. To evaluate the ability of PFNs to kill malarial parasites, the PDI effect of PFNs was evaluated within the infected erythrocytes. Furthermore, malarial parasites were completely eradicated from the erythrocytes after PDI treatment using PFNs on the basis of an 8 day erythrocyte culture test.

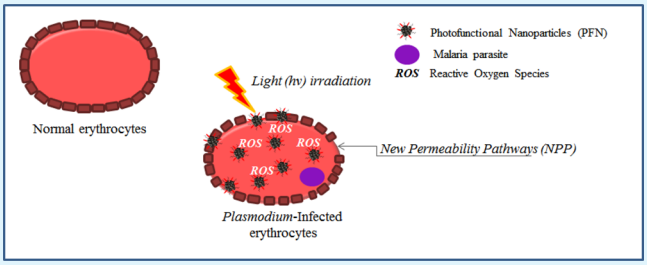

KEYWORDS: *photofunctional nanoparticles, photodynamic inactivation, reactive oxygen species, Plasmodium, malaria, Plasmodium-infected erythrocytes*

INTRODUCTION

Malaria is a mosquito-borne disease caused by Plasmodium species and is responsible for approximately 800 000 deaths a year worldwide.[1] The malaria epidemic is mediated by Plasmodium-infected mosquitoes; the parasite is transmitted to the human host after a blood meal; in the human host, the malarial protozoans parasitize erythrocytes and reproduce through self-replication.[2,3]

Various antimalarial drugs have been developed for the treatment of malaria,[4] such as antifolates, which suppress the synthesis of folic acid, which is essential for the proliferation of Plasmodium.[1,5] However, these drugs have lost their efficacy due to the emergence of drug-resistant Plasmodium strains induced by overuse of quinolones and antifolates.[6,7] Several research groups have recently reported the treatment of drug-resistance bacteria using the photodynamic therapy (PDT).[8−10] In PDT, reactive oxygen species are generated through charge-transfer and/or energy-transfer processes from a photoexcited photosensitizer and induce apoptosis or necrosis of harmful organisms by oxidation and/or activation of the signaling pathways.[11−15] Baptista and colleagues showed that PDT could be used to treat various tropical diseases, including malaria.[8,12] However, because general PDI agents can be taken up by noninfected erythrocytes, this method has limited practical application.[16]

In this study, we report enhanced photodynamic inactivation (PDI) of Plasmodium-infected erythrocytes by photofunctional nanoparticles (PFNs) and maintenance of the PDI effect of PFN over an extended period of time.

EXPERIMENTAL METHODS

Fabrication of PFNs. Magnetic nanoparticles (MNPs) were fabricated using the solvothermal reduction method reported previously.[17] $FeCl_3{\cdot}6H_2O$ (98%), pheophorbide A (PA; 99%),

Received: December 30, 2016
Accepted: March 29, 2017
Published: March 29, 2017

DOI: 10.1021/acsami.6b16793
ACS Appl. Mater. Interfaces 2017, 9, 12975−12981

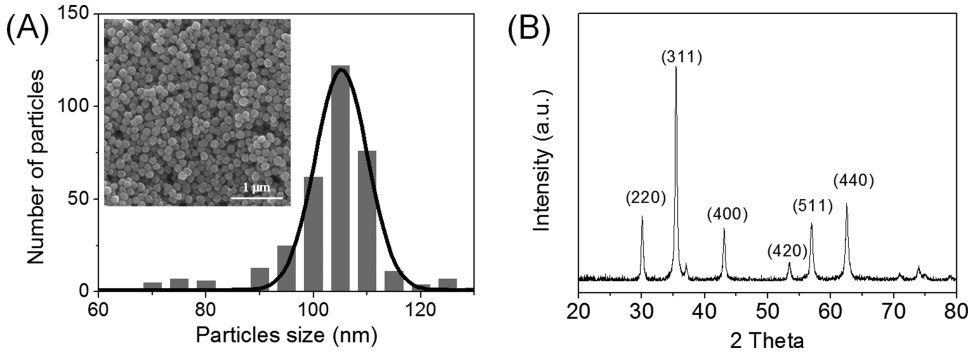

Figure 1. (A) Particle-size distribution of MNPs and SEM image (inset). (B) XRD pattern of MNPs.

polyethylene glycol (PEG; MW 1305−1595), ethylene glycol (EG; 99%), and NaAc (99%) were purchased from Sigma-Aldrich and used without further purification. $FeCl_3 \cdot 6H_2O$ (1.35 g, 5 mmol) and PEG (1.0 g) were completely dissolved in EG (40 mL), and then, NaAc (4.69 g) was added to the mixture under vigorous stirring (200 rpm) at 60 °C for 30 min. The viscous slurry was transferred into a Teflon bottle in a solvothermal autoclave reactor.[18,19] The autoclave was heated and maintained at 200 °C for 12 h and then allowed to cool to room temperature. Precipitates were collected after washing with ethanol five times and were dried at 60 °C for 6 h. To fabricate PFNs by the esterification reaction, MNPs (10 mg) were dispersed in the PA solution (10 mL, 1.76×10^{-5} M in tetrahydrofuran (THF)). This solution was agitated (200 rpm) at room temperature. After 24 h, the product was washed with the THF solvent three times and then dried at 60 °C for 6 h.[17]

Instrumentation. Field-emission scanning electron microscopy (FE-SEM; JSM-6701F; Jeol Ltd.) was utilized to study the morphology of the MNPs. The crystallographic structure of the nanoparticles was investigated by X-ray diffractometry (XRD; Rigaku, ultima IV) using Cu Kα radiation. Fabrication of PFNs was confirmed by Fourier transform infrared (FT-IR) spectroscopy using an FT-IR spectrophotometer (Impact 400; Nicolet). Steady-state absorption and emission spectra were obtained with a UV−vis spectrophotometer (U-2900; Hitachi) and a spectrofluorimeter (F-4500; Hitachi), respectively. The Nd-YAG (surelite II-10, 10 Hz, 7 ns; Continuum)-pumped optical parametric oscillator laser (OPO plus, 5 ns; Continuum) was utilized as the excitation source (λ_{ex} = 668 nm) for the detection of time-resolved singlet oxygen phosphorescence. The phosphorescence signal was collected with a near-infrared photomultiplier tube (H10330A; Hamamatsu) at an angle perpendicular to the excitation beam through cutoff (<1000 nm; CVI) and interference filters (1270 nm; Spectrogon). The signal was amplified and acquired by an amplifier (SR445A; Stanford Research Systems) and a 500 MHz digital oscilloscope (DS07052A; Agilent Technology) and transferred to a computer for further analysis.[20,21]

Biological Assays. The light source for irradiation of PFNs was a light-emitting diode (LED, λ_{max} = 667 nm, full width at half-maximum (FWHM) = 79.6 nm, 6.58 mW/cm^2). LED light was radiated onto the PFNs through a cutoff filter (<400 nm; CVI) to block the residual UV light of the LED. The power density of the LED light at the sample position was measured with a power meter (PM200; Thorlabs). To evaluate the PDI efficiency of the PFNs, erythrocytes and *Plasmodium falciparum* strain 3D7 (chloroquine-susceptible strain) were used. Complete media consisted of Roswell Park Memorial Institute (RPMI) 1640 supplemented with hypoxanthine, $NaHCO_3$, human plasma, gentamicin, and AlbuMAX I. To infect the erythrocytes, erythrocytes (45.5×10^6 cell/mL) were cultured with *P. falciparum* 3D7 in complete media under a mixed gas phase ($O_2/CO_2/N_2$ = 5:5:90) at 37 °C for 3 weeks.[22] Infection of erythrocytes was evaluated by Giemsa staining.[23] Of the erythrocytes, 10% were infected with *P. falciparum* 3D7. The Plasmodium-infected erythrocytes were cultured in the dark with various concentrations of PFNs (0−100 μg/mL) for toxicity testing and were also cultured without PFNs under various light-irradiation conditions (LED, λ_{max} = 667 nm, FWHM = 79.6 nm, 6.58 mW/cm^2, 0−120 min) to test for light toxicity. The PFNs were incubated with infected erythrocytes at room temperature for 24 h in the dark to allow uptake. To evaluate the intracellular uptake efficiency of PA and PFNs, PA (0.16 μM) and PFNs (25 μg/mL) were incubated with Plasmodium-infected erythrocytes for 60 min at 37 °C. The presence of PA and PFNs in the Plasmodium-infected erythrocytes was assessed using a fluorescence microscope (iXon EMCCD; Andor) and flow cytometric analysis (NAVIOS; Beckman Coulter). In the case of flow cytometric analysis, RBCs were gated on the basis of their forward scatter and side scatter signals with logarithmic scales. At least 50 000 particles were assessed and plotted in two-dimensional scattergrams of two of these three parameters, FSC, SSC, and FL4 (Fluorescence Detector 4 (680−710 nm emission)). PA and PFNs were detected in RBC areas with fluorescence (FL2). The RBC area, PA area, and PFNs were detected by analyzing the scattergrams from the computer software.

PDI and Eradication of Plasmodium from Erythrocytes. PDI experiments were performed with various concentrations of PA and PFN. The amount of PA molecules bonded to the surface of the magnetic particles was estimated using UV−vis absorption spectroscopy. Absorption optical densities (O.D.'s) at 667 nm were measured with the initial PA/THF solution (1.85×10^{-5} M) before the addition of magnetic particles for reaction and also with the PA/THF solution that remained after reaction with the particles. The O.D. difference between the initial and remaining PA/THF solutions indicated that ~6.49×10^{-8} mol (equivalent to 3.9×10^{16} molecules) of PA was immobilized onto the surface of 10 mg of magnetic particles. Therefore, the number of PA molecules bonded to the surface of the magnetic particles at 25, 50, 75, and 100 μg/mL of PFN was equivalent to the number of PA molecules in the liquid solution at concentrations of 0.16, 0.32, 0.48, and 0.65 μM, respectively. In experiments comparing PA and PFNs, the number of PA molecules applied was kept the same. The applied concentrations were 0−0.65 μM PA and 0−100 μg/mL PFNs. Plasmodium-infected erythrocytes that were treated with PA or PFN were cultured for 24 h and then placed in culture flasks under light irradiation with an LED (λ_{max} = 667 nm, FWHM = 79.6 nm, 6.58 mW/cm^2) for 30 min. After 48 h, the number of infected cells was estimated by Giemsa staining[23] and the Plasmodium real-time polymerase chain reaction (RT-PCR) assay. Eradication of the parasite was validated by evaluating Plasmodium proliferation after 8 days of culture of the Plasmodium-infected erythrocytes treated with PDI. The target genes of the RT-PCR were circumsporozoite protein (CSP) and plasmodium lactate dehydrogenase (pLDH) genes of *P. falciparum*. Plasmodium DNAs were extracted from 100 μL of the PDI-treated samples using the QIAamp DNA Mini Kit (Qiagen, Hilden, Germany). Briefly, each tube contained a 25 μL reaction mix, which included 2.5 μL of isolated DNA, 0.1 μM of forward and reverse primers, and 0.1 μM of the probe. TaqMan amplification and detection were performed with a real-time thermocycler CFX96 (Bio-Rad, Hercules, CA). Thermocycling conditions were initial denaturation at 95 °C for 3 min, followed by 45 cycles at 95 °C for 15 s and 60 °C for 60 s. The RT-PCR analysis indicates that the lower the threshold cycle (C_t) value, the more the number of genes present.

DOI: 10.1021/acsami.6b16793
ACS Appl. Mater. Interfaces 2017, 9, 12975−12981

RESULTS AND DISCUSSION

As shown in Figure 1A, the fabricated MNPs had good size uniformity. The size histogram of MNPs was obtained by sampling 340 particles in different regions of the FE-SEM image. The average particle size was 103 ± 21 nm. The powder XRD pattern of MNPs provided detailed structural information, as shown in Figure 1B. The strong Bragg reflection peaks (2θ = 30.0, 35.6, 43.3, 53.7, 57.0, 62.8°) are marked by their Miller indices ((220), (311), (400), (422), (511), and (440), respectively), which were obtained from standard Fe_3O_4 powder diffraction data (card 19-0629; JCPDS). The position and relative intensity of all diffraction peaks corresponded to the characteristic peaks of a magnetite crystal with a cubic inverse spinel structure.[17,19]

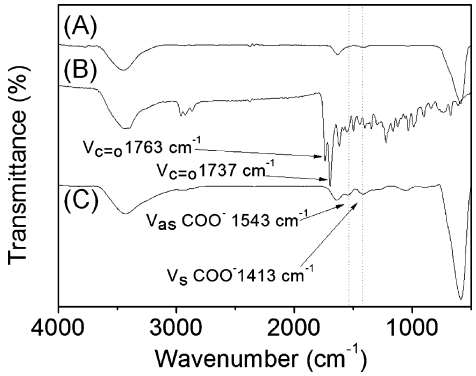

Figure 2. FT-IR spectra of (A) MNPs, (B) PA molecules, and (C) PFNs.

To understand the bonding nature of the carboxyl groups of PA and the Fe ions of MNPs, FT-IR spectra of all samples were compared, as shown in Figure 2. The IR spectrum of PA had absorption peaks at 1763 and 1737 cm^{-1}, which correspond to the stretching modes of the free carbonyl double bond ($\upsilon_{C=O}$) (Figure 2B).[24] After esterification between the carboxyl group of PA and Fe ion of MNPs, the peaks assigned to the free carboxyl group disappeared (1763 and 1737 cm^{-1}) and new bands appeared at 1543 and 1413 cm^{-1}, which we ascribed to the asymmetric (υ_{as}) and symmetric (υ_s) stretch vibrations of the carboxylate group (COO—), respectively.[24] The appearance of these new bands was also reported in the IR study of Dravid and colleagues.[25] This pattern of spectral change is due to Fe−carboxylate complexation as a result of chemical coordination, as shown previously.[26]

The photophysical properties of PFNs were characterized by steady-state absorption and emission spectroscopies. Figure 3A presents the characteristics of PA absorption bands: the Soret band at 410 nm and the Q bands at 504, 534, 608, and 666 nm were nearly identical for PA in THF solution and PFNs in THF solution.[27] The fluorescence emission peaks of PFNs in THF solution at 675 and 725 nm were also similar to those of PA in THF solution (Figure 3B). This suggests that the photophysical properties of PA are not altered by bonding between PA and MNPs.[10]

The most direct measurement method for singlet oxygen is the detection of phosphorescence from the deactivation of singlet oxygen molecules induced by photoexcited PA.[28] As shown in Figure 4, singlet oxygen phosphorescence signals from low concentrations of PA (0.016 μM) and PFNs (2.5 μg/mL) were measured in THF solution at a detection wavelength of 1270 nm to avoid light scattering from the MNPs. The intensities of the singlet oxygen phosphorescence signal at the zero time point were nearly identical for PA and PFNs in THF solution. The phosphorescence decay signals from PA and PFNs were fitted to a single exponential function, yielding similar singlet oxygen lifetimes of 22.7 and 22.1 μs, respectively. These measured singlet oxygen lifetimes are consistent with the reported value.[28] These results indicate that the same amount of singlet oxygen was generated from PA and PFN and that the singlet oxygen generated from PFNs did not undergo self-quenching by the interface modified MNPs.[20,29]

To assess the toxicities of PFNs and irradiated light, Plasmodium-infected erythrocytes were cultured with PFNs in the dark or only with light irradiation in the absence of PFNs. PFNs were not toxic in the concentration range of 0−100 μg/mL, and no light toxicity in the energy range of 0−48 J was evident (see Figure 5).

The PA- and PFN-uptaken RBC counts are quantified as 11.7 and 23.8%, respectively. The more efficient uptake of PFNs compared to that of PA shown in Figure 6B is expected to be due to the enhanced permeability and retention (EPR) effect of the former.[30] The permeability of the erythrocytes increases during malarial infection due to the destruction of the spectrin network.[31] Both PFNs and PAs can be taken up easily by Plasmodium-infected erythrocytes due to the induction of new permeability pathways by the malarial parasite.[32] The uptaken PFNs accumulate in the Plasmodium-infected erythrocytes because of physicochemical pharmacological factors.[16,32]

After 30 min of irradiation for PDI treatment, the infection rate of the erythrocytes decreased in a dose-dependent manner according to the concentrations of PAs and PFNs (Figure 7A).

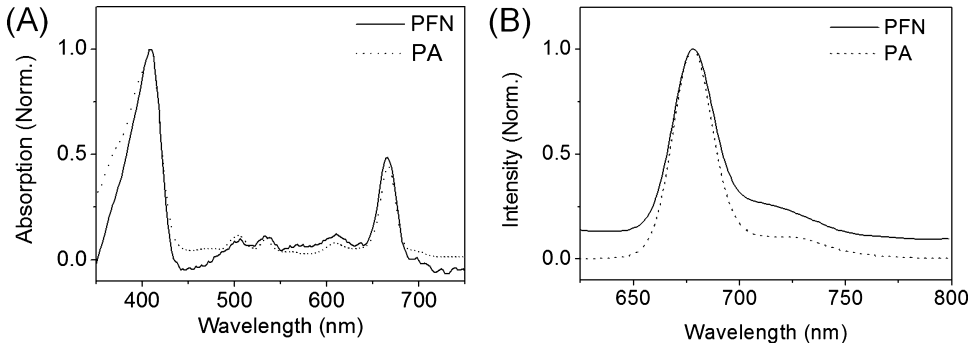

Figure 3. (A) Absorption and (B) emission spectra of pure PA and PFNs in THF. The excitation wavelength for the emission spectrum was 410 nm.

DOI: 10.1021/acsami.6b16793
ACS Appl. Mater. Interfaces 2017, 9, 12975−12981

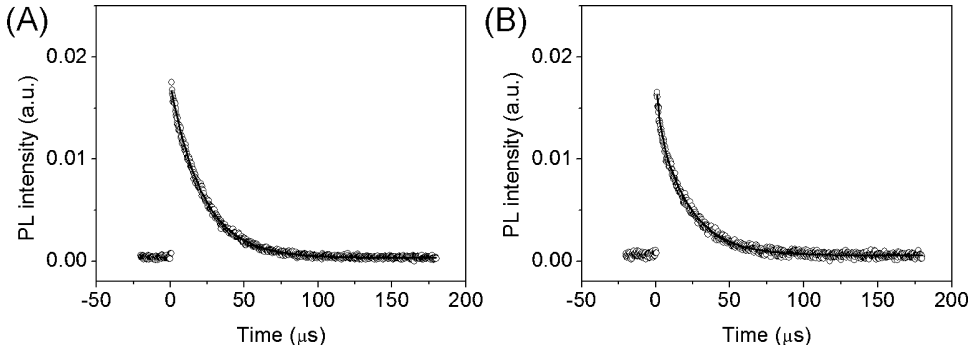

Figure 4. Phosphorescence decay signals induced by relaxation of the singlet oxygen from (A) PA and (B) PFNs in THF solution. Phosphorescence signals were detected at 1270 nm and fitted with a single exponential function (solid line).

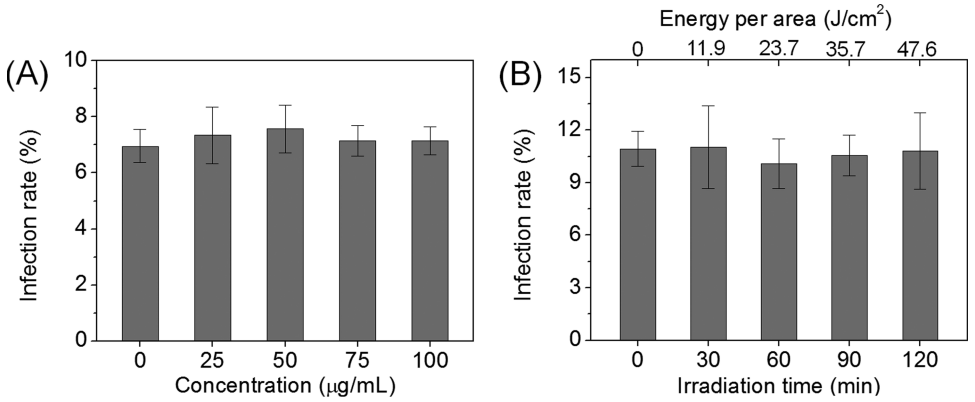

Figure 5. Toxicity test of (A) PFNs without light irradiation and (B) only under light irradiation without PFNs. These experiments were repeated three times.

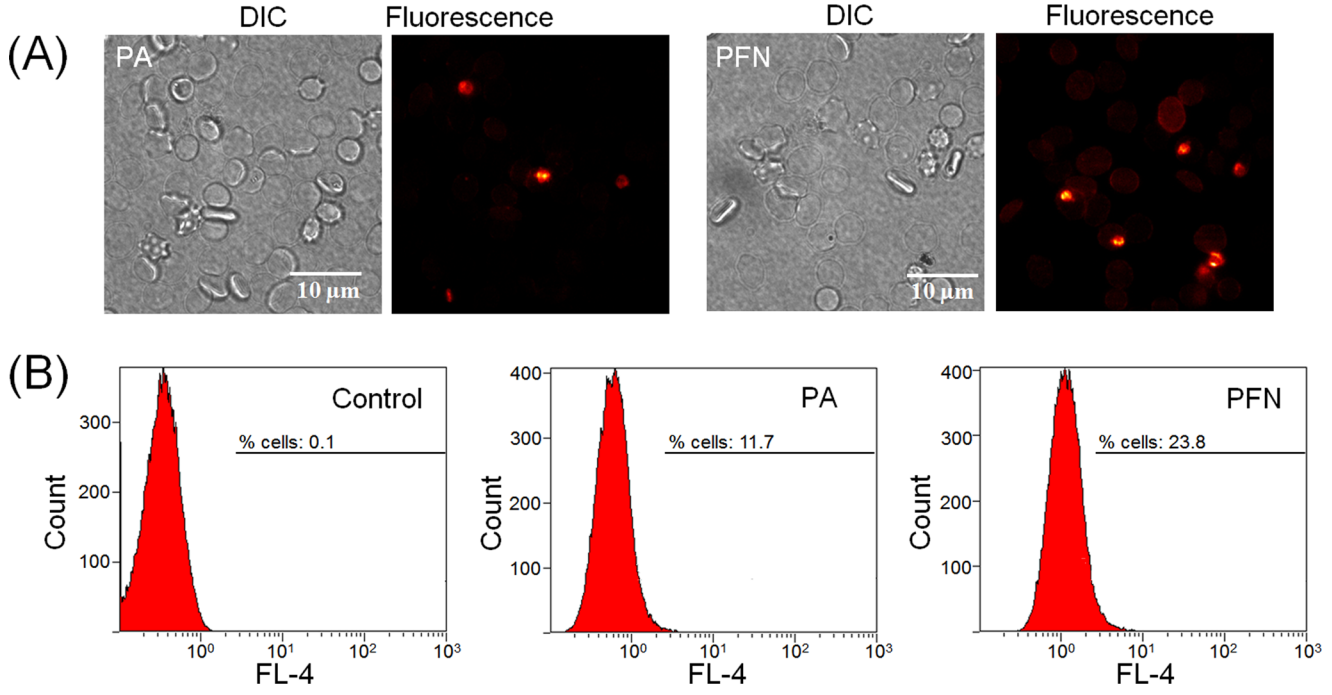

Figure 6. Fluorescence images of PA and PFNs in Plasmodium-infected erythrocytes. (A) Plasmodium-infected erythrocytes were incubated with PA (0.16 μM) or PFNs (25 μg/mL) in a culture medium for 1 h at 37 °C. The uptake efficiencies of PA and PFNs were quantified by flow cytometric analysis (B).

As shown in Figure 7B, there was a difference in the reduction of infection rates between PAs (0.32 μM) and PFNs (50 μg/mL) after irradiation with LED light. The concentration of PA (0.32 μM) was equivalent to the concentration of PA molecules bonded to the surfaces of the PFNs (50 μg/mL). PFNs resulted in a greater reduction in infection during the initial 15 min and

DOI: 10.1021/acsami.6b16793
ACS Appl. Mater. Interfaces 2017, 9, 12975−12981

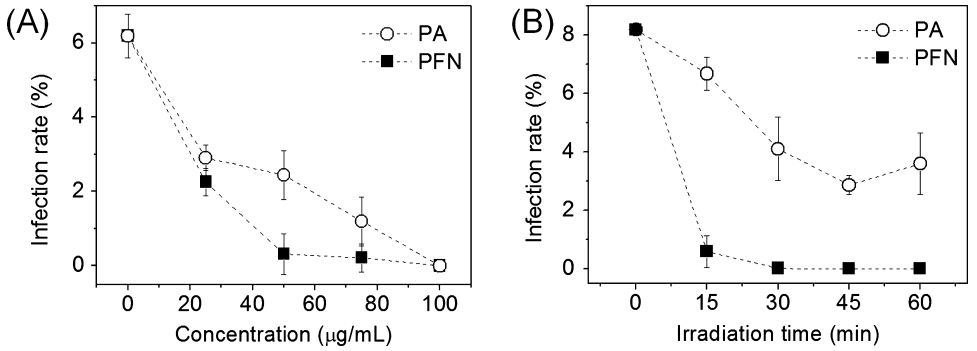

Figure 7. PDI of *P. falciparum* according to (A) the concentration of PDI agents (PAs and PFNs) and (B) LED irradiation time. The experiments were repeated in triplicate.

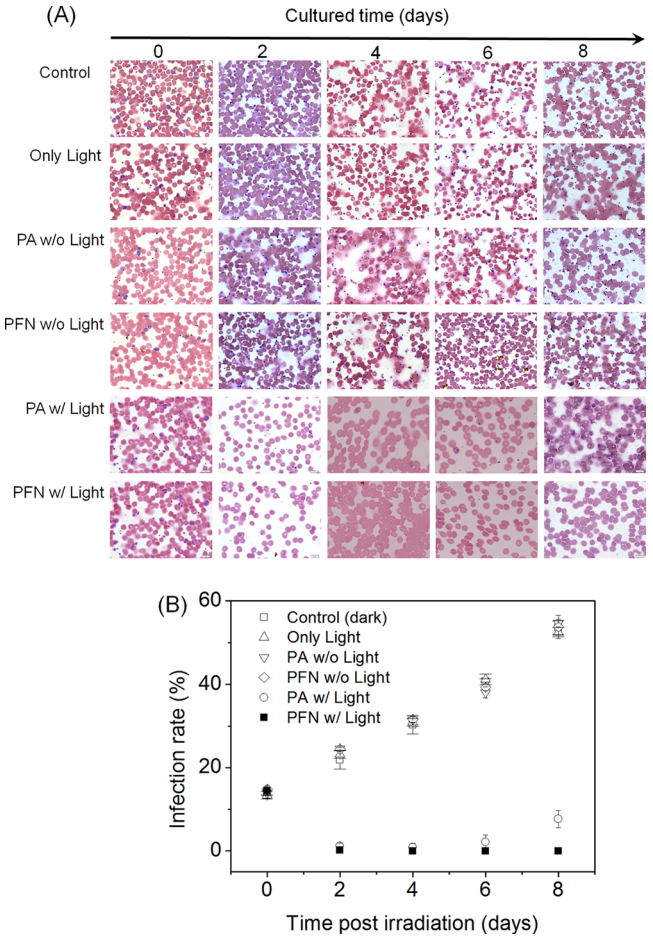

Figure 8. *P. falciparum* eradication at 8 days after PDI treatment. Plasmodium-infected erythrocytes were visualized by Giemsa staining. Magnified stained images of control (dark), only light, PA/PFN without light, and PA-/PFN-mediated PDI treatments are shown in (A). (B) Infection rates were quantified as a function of time. The experiments were repeated in triplicate.

a 0% infection rate after 30 min. In contrast, PA molecules reduced the infection rate to only 56% of that of PFNs over the same time period. This suggests that PFNs are more effective than PAs for PDI treatment of Plasmodium-infected erythrocytes.

The Plasmodium-infected erythrocytes were incubated for 8 more days after only light irradiation for 30 min without PDI agents (PAs or PFNs) and incubated for 8 days with only PA (0.48 μM) or PFNs (75 μg/mL) without light irradiation, and also incubated with PDI treatment for only 30 min of the initial period with PAs (0.48 μM) or PFNs (75 μg/mL). Every 2 days, the proliferation of the malarial parasites was assessed by Giemsa staining and the RT-PCR assay. As shown in Figure 8B, the infection rates of *P. falciparum* were continuously increased in the cases of the light-only condition without the PDI agents and the PDI agents-only condition without irradiation. In the case of PDI treatment with PA, the infection rate increased again after 4 days and the malarial parasite count increased again after 6 days. In contrast, the infection rate did not increase after PDI treatment using PFNs and erythrocyte rupture did not occur (see Figure 8A). In addition, the RT-PCR analysis indicates that the lower the C_t value, the more the number of genes present, as shown in Table 1.

Table 1. Change of the C_t Values of the *P. falciparum* CSP Gene and pLDH Gene by RT-PCR[a]

gene	treatment	0 days	2 days	4 days	6 days	8 days
P.f.[b] *CSP*[c] gene	control	27.33	29.61	29.62	28.42	24.88
	PA	27.13	33.39	33.8	31.67	29.41
	PFNs	28.5	N/A	N/A	N/A	N/A
P.f. *pLDH*[d] gene	control	27.51	30.12	30.24	28.87	25.06
	PA	27.67	34.04	34.35	32.39	30.09
	PFNs	27.52	N/A	N/A	N/A	N/A

[a]Control, PAs, and PFNs represent the light-only condition without PDI agents and the conditions of PDI treatments with PA and PFNs, respectively. [b]*P. falciparum*. [c]Circumsporozoite protein. [d]Plasmodium lactate dehydrogenase.

CONCLUSIONS

We fabricated MNPs coupled to PA molecules using a simple modification process. The fabricated PFNs were characterized by SEM, XRD, FT-IR, absorption spectroscopy, and emission spectroscopy. The PFNs generated singlet oxygens, as confirmed by time-resolved near-IR spectroscopy. A comparison of PDI treatment with PAs and PFNs showed that Plasmodium-infected erythrocytes were more effectively treated with PFN/PDI than with PA/PDI due to the EPR effect of PFNs. More importantly, PDI treatment with PFNs eradicated the malarial parasite from the erythrocytes without recurrence after 8 days.

AUTHOR INFORMATION

Corresponding Authors

*E-mail: malarim@korea.ac.kr. Tel: +82-2626-3245. Fax: +82-2-2626-1465 (C.S.L.).

DOI: 10.1021/acsami.6b16793
ACS Appl. Mater. Interfaces 2017, 9, 12975−12981

*E-mail: yrkim@yonsei.ac.kr. Tel: +82- 2123-2646. Fax: +82-2-364-7050 (Y.-R.K.).

ORCID

Yong-Rok Kim: 0000-0001-8166-9889

Author Contributions

‖K.-K.W., J.W.J., E.P.S., and H.Y.S. contributed equally to this manuscript.

Author Contributions

All authors contributed to the writing of this manuscript and have approved the final version of the manuscript.

Notes

The authors declare no competing financial interest.

■ ACKNOWLEDGMENTS

This work was carried out with the support of the "Cooperative Research Program for Agriculture Science & Technology Development (Project No. PJ01083001)" Rural Development Administration, Republic of Korea, and by a grant from the National Research Foundation (NRF) of Korea, funded by the Korea government (MSIP) (No. NRF-2016R1A2B4011155).

■ REFERENCES

(1) LeBlanc, D.; Story, R.; Gross, E. Laser-Induced Inactivation of *Plasmodium falciparum*. *Malar. J.* **2012**, *11*, 267.

(2) Maier, A. G.; Cooke, B. M.; Cowman, A. F.; Tilley, L. Malaria Parasite Proteins That Remodel the Host Erythrocyte. *Nat. Rev. Microbiol.* **2009**, *7*, 341−354.

(3) Augustine, A. D.; Hall, B. F.; Leitner, W. W.; Mo, A. X.; Wali, T. M.; Fauci, A. S. Niaid Workshop on Immunity to Malaria: Addressing Immunological Challenges. *Nat. Immunol.* **2009**, *10*, 673−678.

(4) Sidhu, A. B. S.; Verdier-Pinard, D.; Fidock, D. A. Chloroquine Resistance in *Plasmodium falciparum* Malaria Parasites Conferred by pfcrt Mutations. *Science* **2002**, *298*, 210−213.

(5) Chango, A.; Abdennebi-Najar, L. Folate Metabolism Pathway and *Plasmodium falciparum* Malaria Infection in Pregnancy. *Nutr. Rev.* **2011**, *69*, 34−40.

(6) Ridley, R. G. Medical Need, Scientific Opportunity and the Drive for Antimalarial Drugs. *Nature* **2002**, *415*, 686−693.

(7) Le Bras, J.; Durand, R. The Mechanisms of Resistance to Antimalarial Drugs in *Plasmodium falciparum*. *Fundam. Clin. Pharmacol.* **2003**, *17*, 147−153.

(8) Zhao, X.-J.; Lustigman, S.; Kenney, M. E.; Ben-Hur, E. Structure-Activity and Mechanism Studies on Silicon Phthalocyanines with *Plasmodium falciparum* in the Dark and under Red Light. *Photochem. Photobiol.* **1997**, *66*, 282−287.

(9) Kashef, N.; Abadi, G. R. S.; Djavid, G. E. Phototoxicity of Phenothiazinium Dyes against Methicillin-Resistant *Staphylococcus aureus* and Multi-Drug Resistant *Escherichia coli*. *Photodiagn. Photodyn. Ther.* **2012**, *9*, 11−15.

(10) Huang, P.; Li, Z. M.; Lin, J.; Yang, D. P.; Gao, G.; Xu, C.; Bao, L.; Zhang, C. L.; Wang, K.; Song, H.; Hu, H. Y.; Cui, D. X. Photosensitizer-Conjugated Magnetic Nanoparticles for in Vivo Simultaneous Magnetofluorescent Imaging and Targeting Therapy. *Biomaterials* **2011**, *32*, 3447−3458.

(11) Hajri, A.; Wack, S.; Meyer, C.; Smith, M. K.; Leberquier, C.; Kedinger, M.; Aprahamian, M. In Vitro and in Vivo Efficacy of Photofrin (R) and Pheophorbide A, a Bacteriochlorin, in Photodynamic Therapy of Colonic Cancer Cells. *Photochem. Photobiol.* **2002**, *75*, 140−148.

(12) Baptista, M. S.; Wainwright, M. Photodynamic Antimicrobial Chemotherapy (Pact) for the Treatment of Malaria, Leishmaniasis and Trypanosomiasis. *Braz. J. Med. Biol. Res.* **2011**, *44*, 1−10.

(13) Zhou, Z.; Song, J.; Nie, L.; Chen, X. Reactive Oxygen Species Generating Systems Meeting Challenges of Photodynamic Cancer Therapy. *Chem. Soc. Rev.* **2016**, *45*, 6597−6626.

(14) Shi, S.; Liu, Y.; Chen, Y.; Zhang, Z.; Ding, Y.; Wu, Z.; Yin, J.; Nie, L. Versatile Ph-Response Micelles with High Cell-Penetrating Helical Diblock Copolymers for Photoacoustic Imaging Guided Synergistic Chemo-Photothermal Therapy. *Theranostics* **2016**, *6*, 2170−2182.

(15) Liu, Y.; Kang, N.; Lv, J.; Zhou, Z. J.; Zhao, Q. L.; Ma, L. C.; Chen, Z.; Ren, L.; Nie, L. M. Deep Photoacoustic/Luminescence/Magnetic Resonance Multimodal Imaging in Living Subjects Using High-Efficiency Upconversion Nanocomposites. *Adv. Mater.* **2016**, *28*, 6411−6419.

(16) Yin, T.; Huang, P.; Gao, G.; Shapter, J. G.; Shen, Y.; Sun, R.; Yue, C.; Zhang, C.; Liu, Y.; Zhou, S.; Cui, D. Superparamagnetic Fe3o4-Peg2k-Fa@Ce6 Nanoprobes for in Vivo Dual-Mode Imaging and Targeted Photodynamic Therapy. *Sci. Rep.* **2016**, *6*, No. 36187.

(17) Choi, K. H.; Lee, H. J.; Park, B. J.; Wang, K. K.; Shin, E. P.; Park, J. C.; Kim, Y. K.; Oh, M. K.; Kim, Y. R. Photosensitizer and Vancomycin-Conjugated Novel Multifunctional Magnetic Particles as Photoinactivation Agents for Selective Killing of Pathogenic Bacteria. *Chem. Commun.* **2012**, *48*, 4591−4593.

(18) Deng, H.; Li, X. L.; Peng, Q.; Wang, X.; Chen, J. P.; Li, Y. D. Monodisperse Magnetic Single-Crystal Ferrite Microspheres. *Angew. Chem., Int. Ed.* **2005**, *44*, 2782−2785.

(19) Huang, Y. N.; Zhang, L. P.; Huan, W. W.; Liang, X. J.; Liu, X. N.; Yang, Y. X. A Study on Synthesis and Properties of Fe3o4 Nanoparticles by Solvothermal Method. *Glass Phys. Chem.* **2010**, *36*, 325−331.

(20) Choi, K. H.; Wang, K. K.; Shin, E. P.; Oh, S. L.; Jung, J. S.; Kim, H. K.; Kim, Y. R. Water-Soluble Magnetic Nanoparticles Functionalized with Photosensitizer for Photocatalytic Application. *J. Phys. Chem. C* **2011**, *115*, 3212−3219.

(21) Wang, K. K.; Jung, M. S.; Choi, K. H.; Shin, H. W.; Oh, S. I.; Im, J. E.; Kim, D. H.; Kim, Y. R. Fabrication and Photophysical Properties of Singlet Oxygen Generating Nanoporous Membrane. *Surf. Coat. Technol.* **2011**, *205*, 3905−3908.

(22) Stanisic, D. I.; Liu, X. Q.; De, S. L.; Batzloff, M. R.; Forbes, T.; Davis, C. B.; Sekuloski, S.; Chavchich, M.; Chung, W.; Trenholme, K.; McCarthy, J. S.; Li, T.; Sim, B. K. L.; Hoffman, S. L.; Good, M. F. Development of Cultured *Plasmodium falciparum* Blood-Stage Malaria Cell Banks for Early Phase in Vivo Clinical Trial Assessment of Anti-Malaria Drugs and Vaccines. *Malar. J.* **2015**, *14*, 143−10.

(23) Sathpathi, S.; Mohanty, A. K.; Satpathi, P.; Mishra, S. K.; Behera, P. K.; Patel, G.; Dondorp, A. M. Comparing Leishman and Giemsa Staining for the Assessment of Peripheral Blood Smear Preparations in a Malaria-Endemic Region in India. *Malar. J.* **2014**, *13*, 512.

(24) Drmota, A.; Kosak, A.; Znidarsic, A. A Mechanism for the Adsorption of Carboxylic Acids onto the Surface of Magnetic Nanoparticles. *Mater. Technol.* **2008**, *42*, 79−83.

(25) Wu, N. Q.; Fu, L.; Su, M.; Aslam, M.; Wong, K. C.; Dravid, V. P. Interaction of Fatty Acid Monolayers with Cobalt Nanoparticles. *Nano Lett.* **2004**, *4*, 383−386.

(26) Jacintho, G. V. M.; Brolo, A. G.; Corio, P.; Suarez, P. A. Z.; Rubim, J. C. Structural Investigation of Mfe2o4 (M = Fe, Co) Magnetic Fluids. *J. Phys. Chem. C* **2009**, *113*, 7684−7691.

(27) Nafiujjaman, M.; Revuri, V.; Nurunnabi, M.; Cho, K. J.; Lee, Y. K. Photosensitizer Conjugated Iron Oxide Nanoparticles for Simultaneous in Vitro Magneto-Fluorescent Imaging Guided Photodynamic Therapy. *Chem. Commun.* **2015**, *51*, 5687−5690.

(28) Wang, K.-K.; Li, J.; Kim, B.-J.; Lee, J.-H.; Shin, H.-W.; Ko, S.-H.; Lee, W.-Y.; Lee, C.-H.; Jung, S. H.; Kim, Y.-R. Photophysical Properties of Pheophorbide-a Derivatives and Their Photodynamic Therapeutic Effects on a Tumor Cell Line in Vitro. *Int. J. Photoenergy* **2014**, *2014*, 1−7.

(29) Paonessa, R. S.; Trogler, W. C. Solvent-Dependent Reactions of Carbon-Dioxide with a Platinum(Ii) Dihydride - Reversible Formation of a Platinum(Ii) Formatohydride and a Cationic Platinum(Ii) Dimer, [Pt2H3(PEt3)4][HCO2]. *J. Am. Chem. Soc.* **1982**, *104*, 3529−3530.

(30) Prabhakar, U.; Maeda, H.; Jain, R. K.; Sevick-Muraca, E. M.; Zamboni, W.; Farokhzad, O. C.; Barry, S. T.; Gabizon, A.; Grodzinski, P.; Blakey, D. C. Challenges and Key Considerations of the Enhanced

DOI: 10.1021/acsami.6b16793
ACS Appl. Mater. Interfaces 2017, 9, 12975−12981

Permeability and Retention Effect for Nanomedicine Drug Delivery in Oncology. *Cancer Res.* **2013**, *73*, 2412−2417.
(31) Shi, H.; Liu, Z.; Li, A.; Yin, J.; Chong, A. G.; Tan, K. S.; Zhang, Y.; Lim, C. T. Life Cycle-Dependent Cytoskeletal Modifications in *Plasmodium falciparum* Infected Erythrocytes. *PLoS One* **2013**, *8*, No. e61170.
(32) Santos-Magalhães, N. S.; Mosqueira, V. C. Nanotechnology Applied to the Treatment of Malaria. *Adv. Drug Delivery Rev.* **2010**, *62*, 560−575.

DOI: 10.1021/acsami.6b16793
ACS Appl. Mater. Interfaces 2017, 9, 12975−12981